REPORT DOCUMENTATION PAGE

AFRL-SR-BL-TR-02-

0137

1. AGENCY USE ONLY (Leave blank)	2. REPORT DATE	3. REPO...
		01 Apr 98 to 30 Sep 01 FINAL

4. TITLE AND SUBTITLE	5. FUNDING NUMBERS
(AASERT 98) Nonequilibrium Air Plasma Chemistry	61103D 3484/TS

6. AUTHOR(S)

Professor Kruger

7. PERFORMING ORGANIZATION NAME(S) AND ADDRESS(ES)	8. PERFORMING ORGANIZATION REPORT NUMBER
Stanford University 496 Lomita Mall Durand Bldg 137 Stanford, CA 94305-4030	

9. SPONSORING/MONITORING AGENCY NAME(S) AND ADDRESS(ES)	10. SPONSORING/MONITORING AGENCY REPORT NUMBER
AFOSR/NE 801 North Randolph Street Rm 732 Arlington, VA 22203-1977	F49620-98-1-0425

11. SUPPLEMENTARY NOTES

12a. DISTRIBUTION AVAILABILITY STATEMENT	12b. DISTRIBUTION CODE
APPROVAL FOR PUBLIC RELEASED; DISTRIBUTION UNLIMITED	

13. ABSTRACT (Maximum 200 words)

This AASERT program has enabled the training and support of four graduate students (Richard Gessman, PhD. 1999, Edward Wahl, Ph.D. 2000, Kate Snyder, Ph.D. 2002, expected, and Jonathan Flad, Ph.D. 2002, expected) in the framework of the Air Plasma Ramparts MURI program entitled "Mechanism of Ionizational Nonequilibrium in Air Plasmas."

20020419 175

14. SUBJECT TERMS			15. NUMBER OF PAGES
			16. PRICE CODE

17. SECURITY CLASSIFICATION OF REPORT	18. SECURITY CLASSIFICATION OF THIS PAGE	19. SECURITY CLASSIFICATION OF ABSTRACT	20. LIMITATION OF ABSTRACT
UNCLASSIFIED	UNCLASSIFIED	UNCLASSIFIED	UL
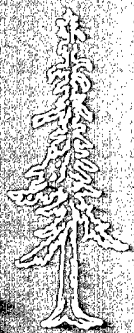
NONEQUILIBRIUM AIR PLASMA CHEMISTRY

Submitted by

Professor Charles H. Kruger
Principal Investigator

March 2002

Mechanical Engineering Department
Stanford University
Stanford, California 94305

1. Contents

Section   **Page**

2. Objectives

This AASERT program has enabled the training and support of four graduate students (Richard Gessman, Ph.D. 1999, Edward Wahl, Ph.D. 2000, Kate Snyder, Ph.D. 2002, expected, and Jonathan Flad, Ph.D. 2002, expected) in the framework of the Air Plasma Ramparts MURI program entitled "Mechanisms of Ionizational Nonequilibrium in Air Plasmas," with Prof. Charles H. Kruger as the Principal Investigator and Dr. Robert J. Barker (AFOSR) as Technical Monitor.

The goal of the Air Plasma Ramparts program is to investigate energy efficient methods for creating and sustaining large volume atmospheric air plasmas with electron number densities greater than 10^{13} cm^{-3} that can be employed to shield aircrafts or other sensitive components from electromagnetic radiation. Our approach at Stanford University has been to enhance ionizational nonequilibrium by means of applied electrical discharges. Our investigations have focused on two types of discharge, namely direct-current (dc) and repetitively pulsed discharges. The AASERT students involved with this program have provided support in the study of the dc discharges in air and nitrogen plasmas. The outcome of this work is presented in the following section.

3. Accomplishments/New Findings

We first describe our two-temperature chemical kinetic models of air plasma discharges. The influence of departures from a Maxwellian distribution of the free-electrons are examined with a simplified collisional-radiative model coupled with a Boltzmann solver for a nitrogen plasma. We then present results of experiments in atmospheric pressure air and nitrogen, using either cold or preheated process gas, in which the electron density was raised to above 10^{12} cm^{-3} by means of a DC discharge. The modeling and experimental results obtained with these DC discharges have led us to design pulsed discharge experiments in which electron densities of more than 10^{12} cm^{-3} in air are produced with approximately 12 W/cm^3, a factor 250 times lower than the power required for a DC discharge.

3.1. Two-Temperature Kinetic Models

Two-temperature chemical kinetic models were developed to understand the mechanisms governing ionization and electron recombination in discharges produced by an applied electric field. The two temperatures are the electron temperature, T_e, and the gas temperature, T_g. Rate coefficients describing the air plasma chemistry were derived using the Weighted Rate Coefficient (WRC) method presented in ref. 2. In this method, rate coefficients are calculated as a weighted average of elementary rates over the internal states of atoms and molecules. Elementary rate coefficients are calculated from cross-

section data assuming Maxwellian velocity distribution functions for electrons and heavy-particles, and are then averaged over the internal energy levels, assuming Boltzmann distributions at the electronic temperature T_{el}, vibrational temperature T_v, and rotational temperature T_r. It is further assumed that $T_{el} = T_e$ and $T_r = T_g$. The remaining parameter, T_v, can only be determined by means of a collisional-radiative (CR) model of vibrationally-specific state-to-state kinetics. We have developed a CR model to determine the relation between T_v and T_g and T_e in atmospheric pressure nitrogen plasmas (ref. 3). It was shown (ref. 4) that the steady-state concentrations determined with a two-temperature kinetic model assuming that $T_v = T_g$ are in close agreement with the CR model predictions in the range of electron densities of interest here, and are at worse within a factor 5 of the CR model predictions at electron densities greater than about 10^{17} cm^{-3} (region B in Fig. 1). In contrast, the often-used assumption $T_v = T_e$ would produce steady-state electron number densities several orders of magnitude greater than those obtained with the CR model at the electron densities of interest. We extend these results to atmospheric pressure air by calculating all WRC rate coefficients with the assumption $T_v = T_g$. Two-temperature kinetic calculations were made with the CHEMKIN solver (ref. 5) modified to account for two-temperature rates (ref. 6). Electron attachment reactions are neglected because the equilibrium concentrations of O_2^- and O^- are negligible relative to the concentration of electrons in atmospheric pressure air above ~1500 K.

3.2. Two-temperature Chemistry Simulations

We consider first the case of an air plasma in equilibrium at 2000 K and 1 atm at time zero when an elevated electron temperature is instantaneously prescribed, in an idealized way modeling an electrical discharge in a reactor section. Species concentrations are calculated for various electron temperatures while keeping the gas temperature constant at 2000 K. For $T_e \geq 6000$ K, electron-catalyzed ionization reactions become important and the steady-state electron number density increases rapidly with the electron temperature. The small circles in Fig. 1 represent the predicted steady-state electron number densities as a function of the electron temperature in atmospheric pressure air at fixed T_g = 2000 K. An abrupt change in electron density occurs for $T_e \cong 17,000$ K where the predicted steady-state electron number density suddenly increases from ~10^{14} to ~4×10^{17} cm^{-3}.
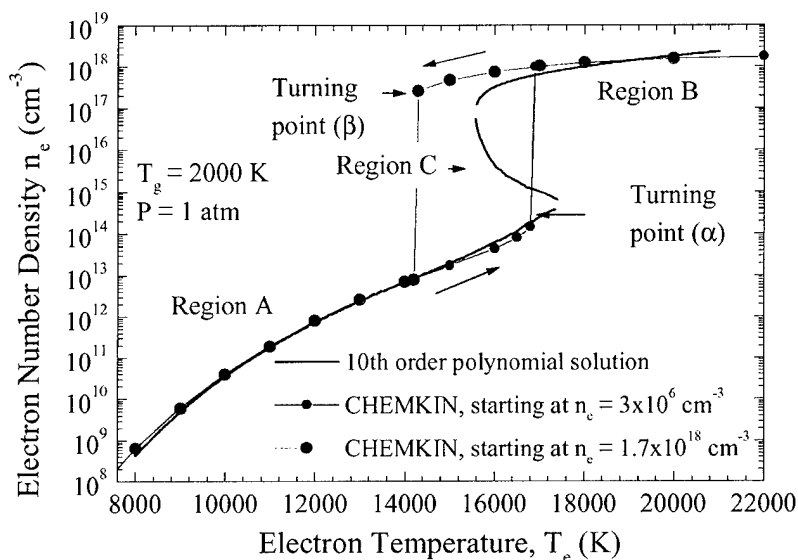
4

Fig. 1. Steady-state electron number densities predicted by CHEMKIN and analytical solution

In the reverse case where steady-state electron concentrations are calculated from an initial composition given by the steady-state solution at $T_g = 2000$ K and $T_e = 22,000$ K (corresponding to $n_e^{(t=0)} \cong 10^{18}$ cm^{-3}), the predicted steady-state electron number densities (large circles in Fig. 1) start by decreasing along the same upper curve as in the previous case, but instead of the abrupt decrease at 17,000 K, continue their smooth decrease until the electron temperature reaches ~14,000 K. When T_e is further decreased below 14,000 K, the steady-state electron density abruptly decreases and then retraces the solution of the previous case. Thus the electron number density as a function of the electron temperature presents a hysteresis. Detailed examinations of the mechanism and rates were made to determine the main reactions controlling the steady-state electron number density in regions A and B (ref. 6):

Region A: When the electric field is applied, the electron concentration rises rapidly as a result of three-body electron-impact ionization of N_2 and O_2 and of electron-impact dissociation of O_2 followed by electron-impact ionization of O. The charged species produced by these processes undergo rapid charge transfer to NO^+, mainly via $O^+ + N_2 \Rightarrow NO^+ + N$. The main electron removal reaction is the two-body dissociative recombination reaction $NO^+ + e \Rightarrow N + O$. When the concentration of NO^+ becomes sufficiently large, the rate of dissociative recombination balances the rate of electron production and the plasma reaches steady-state. Thus in Region A, the termination step of the ionization process is the two-body recombination of a molecular ion.

Region B: The initial electron number density increase occurs by the same processes as in region A, i.e. electron-impact ionization of N_2, O_2, and O. Unlike in Region A, however, charge transfer reactions are not fast enough to produce sufficient NO^+ for the

5

rate of dissociative recombination to balance the ionization rate. This is because the latter reactions are controlled by the gas temperature, whereas electron impact ionization reactions are controlled by T_e. The limit between Regions A and B corresponds approximately to the electron temperature for which the rate of the charge transfer reaction $O^+ + N_2 \Rightarrow NO^+ + N$ is comparable with the rate of avalanche ionization by electron impact. Above this critical electron temperature, the avalanche ionization process continues until all molecular species are dissociated. Eventually the rates of three body electron recombination reactions balance the rate of ionization, and steady-state is reached.

Analytical solution: The kinetics in Regions A and B can be described with a simplified subset of reactions that take into account the dominant channels discussed in the foregoing section. With this simplified mechanism, the steady-state concentrations of major species are obtained by solving the species conservation equations of electrons, O_2, O, NO^+, O^+, O_2^+, and N_2^+. By elimination of n_O, n_{O_2}, n_{O^+}, $n_{O_2^+}$, $n_{N_2^+}$ and n_{NO^+}, a tenth degree polynomial in n_e is obtained, with coefficients that only depend on T_g, T_e, $n_{O2}^{(0)}$ and $n_{N2}^{(0)}$. The roots of this polynomial are plotted in Fig. 1 along with the CHEMKIN predictions obtained with the full kinetic mechanism. As shown in Fig. 1, the analytical solution generally agrees with the CHEMKIN predictions in regions A and B, but it also exhibits an extra solution (Region C) that could not be attained with CHEMKIN. If CHEMKIN is initialized with a point in Region C, a new steady-state electron number density is obtained on either the lower (Region A) or upper (Region B) limb of the steady-state CHEMKIN curves.

3.3. Experimental DC Discharges

For comparison with the kinetic model, the "S-shaped" curves of n_e vs. T_e have been converted into more readily measured current density vs. electric field by use of Ohm's law and the electron energy equation. The latter incorporates the results of the collisional-radiative model to account for non-elastic energy losses from the free electrons to the molecular species. The electrical discharge characteristics of Fig. 4 in the following section exhibit variations that reflect both the S-shaped dependence of electron number density versus T_e, and the dependence of the inelastic energy loss factor on the electron temperature and number density.

To test the predicted S-shaped curve, DC discharge experiments were conducted with low temperature, atmospheric pressure flowing air and nitrogen plasmas. The experimental setup is shown in Fig. 2. Process gas is injected in the discharge region with low initial temperature and electron density. Spectroscopic and electrical measurements are made of the temperature, electrical conductivity and electron density as a function of the applied discharge current.

6
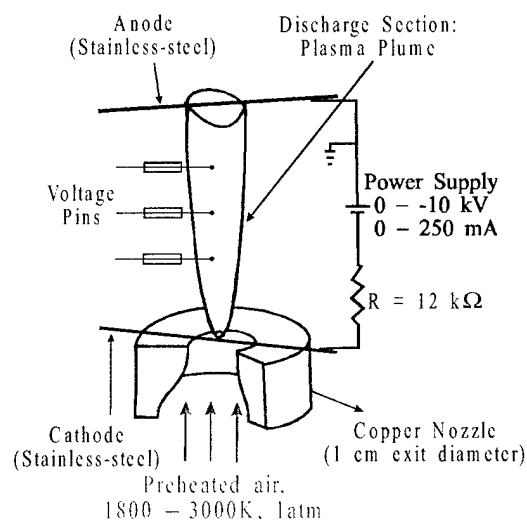
Fig. 2. DC Discharge schematic.

3.3.1. DC Discharge Experiments in Air

Fig. 3a shows a photograph of the air plasma plume at a temperature of approximately 2000 K in the region between the two electrodes without the discharge applied. Fig. 3b shows the same region with a DC discharge of 5.2 kV and 200 mA applied. The interelectrode distance is 3.5 cm. The bright center region in Fig. 3b corresponds to the discharge-excited plasma. The discharge diameter is approximately 3.2 mm (at half-maximum intensity) and the electron concentration determined from electrical conductivity measurements is approximately 10^{12} cm^{-3}. The temperature profile was measured from rotational lines of the OH (A-X) transition in the case without the discharge, and of the N_2 (C-B) transition with the discharge applied. The centerline temperature decreases from 2300 K at the cathode to 2020 K at the anode when no discharge is applied. With the discharge, the measured temperature remains approximately constant at 2300 K along the discharge axis. Radial temperature profiles measured at 1.5 cm downstream of the cathode are shown in Fig. 3c. It appears that the discharge does not noticeably increase the rotational temperature of the plasma under these conditions.
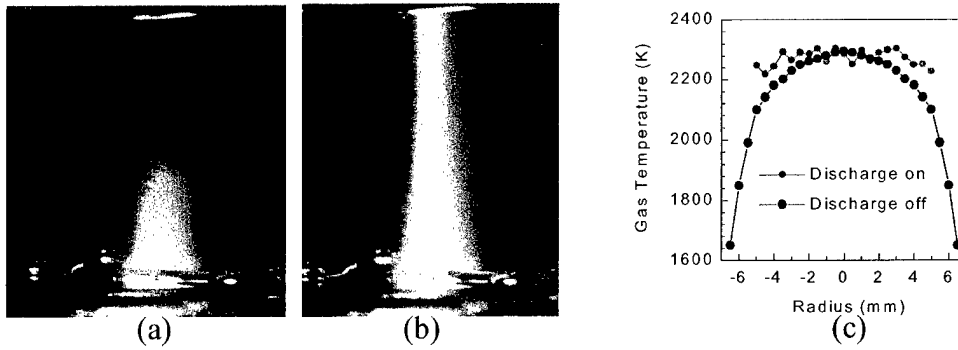
7

Fig. 3. (a) Air plasma at 2000 K without discharge, (b) Air plasma at 2000 K with discharge (1.4 kV/cm, 200 mA). Interelectrode gap: 3.5 cm. Measured electron number density in the discharge region: ~1012 cm-3, (c) Rotational temperature profiles at 1.5 cm above the bottom electrode.

The measured discharge characteristics for plasma temperatures ranging from 1800 to 2900 K are shown in Fig. 4. Also shown are the predicted discharge characteristics at temperatures of 2000 and 3000 K. A more detailed description of our theoretical work on discharge characteristics may be found in ref. 6. Good agreement is obtained between the measured and predicted discharge characteristics over a range of experiments spanning over three orders of magnitude in current density.
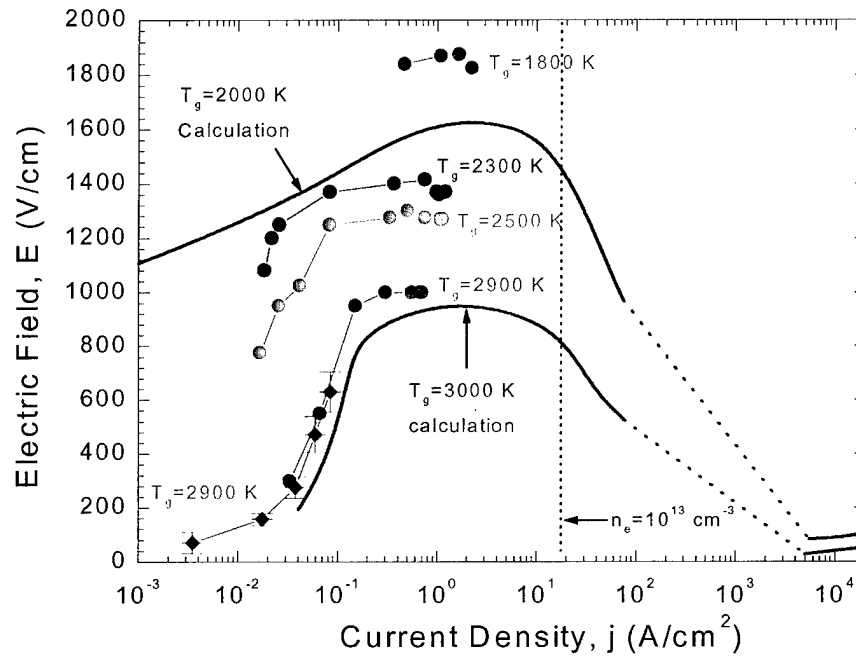

Fig. 4. Measured (symbols) and predicted DC discharge characteristics in air at 1 atm.

3.3.2. Discharge Experiments in Nitrogen

Discharge experiments were also conducted with atmospheric pressure nitrogen either at room temperature or preheated to temperatures between 1800-2250 K. For the

room temperature experiments, nitrogen is injected between the electrodes at a velocity of about 2 m/s. The gas heats up to temperatures between 2200 and 2800 K as a result of discharge-induced Joule heating. For the experiments with preheated nitrogen, the gas is injected at about 450 m/s. Owing to the relatively fast flow rate, the gas temperature remains practically constant in the discharge region. The discharge diameter is about 1.7 mm in the room temperature nitrogen experiments, and 5 mm in preheated nitrogen. The difference in discharge diameters is due to the larger radial thermal gradients in cold nitrogen than in the preheated flow. In all cases the measured cathode fall is about 300 V, which is typical of a glow discharge. The measured discharge characteristics are shown in Fig. 5, along with the characteristics calculated with the nitrogen CR model. As shown in Fig. 5, the measured characteristics support the results of the chemistry and discharge models.

The foregoing calculations were performed using Maxwellian distribution functions for the translational energies of the electrons and heavy particles. To investigate the limitations of this simplification, the electron Boltzmann equation was solved for nitrogen plasmas in conjunction with a somewhat simplified form of the collisional-radiative model. The results, shown in Fig. 6, do not differ significantly from those with the Maxwellian version.
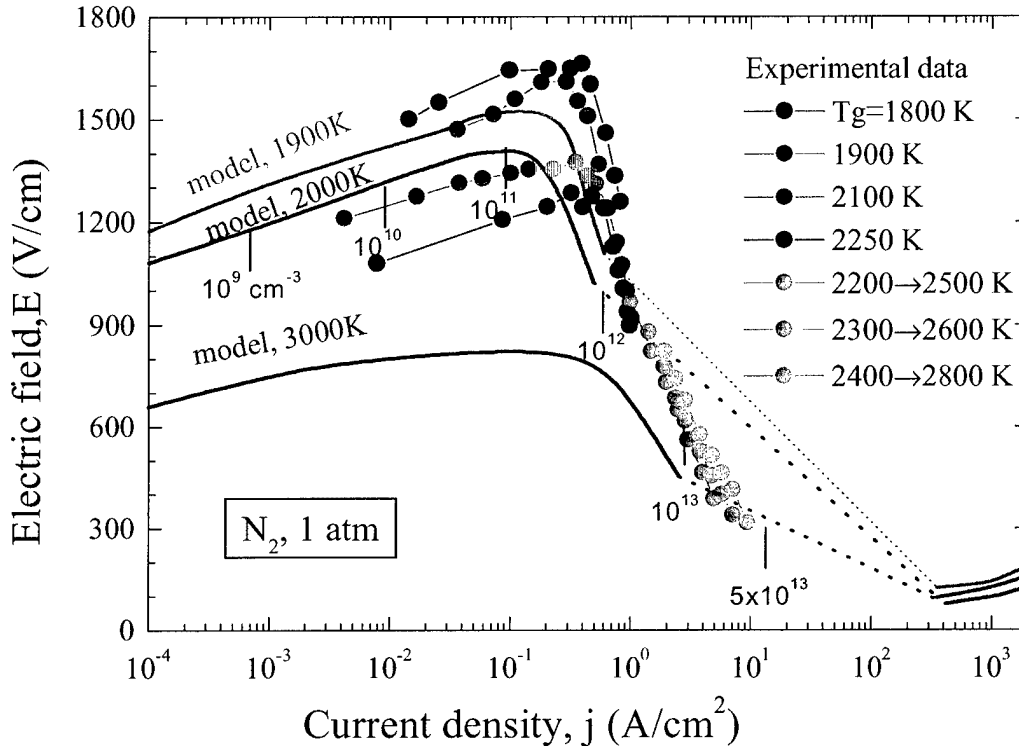

Fig. 5. Measured (symbols) and predicted DC characteristics in nitrogen at 1 atm.
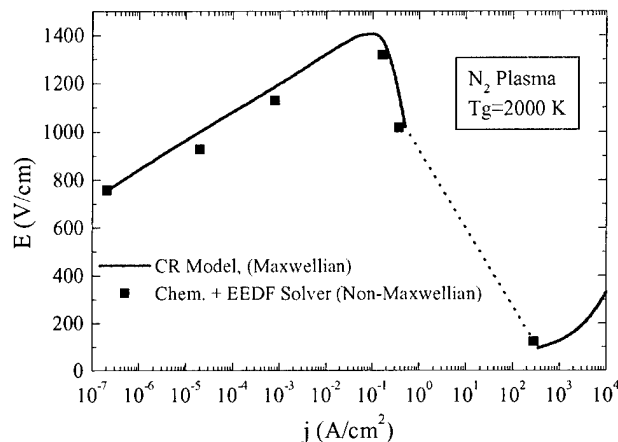
Fig. 6. Predicted discharge characteristics in atmospheric pressure nitrogen at 2000 K.

3.4. Summary and Conclusions

Two-temperature ($T_e > T_g$) kinetic models accounting for ionizational, chemical, vibrational and electronic nonequilibrium, and incorporating a collisional-radiative model with over 11,000 transitions have been developed to understand the mechanisms of ionizational nonequilibrium in atmospheric pressure air and nitrogen electrical discharges. These models predict that (even) at atmospheric pressure energetic electrons driven by the discharge can establish and maintain electron-density nonequilibrium of over six orders of magnitude. An unexpected result is an "S-shaped" dependence of n_e on T_e at steady-state for a given gas temperature. This behavior results from a transition between predominately molecular ions to atomic ions at a critical value of T_e and values of n_e above about 10^{14} cm^{-3}. Above this critical value of T_e, the electron density increases dramatically so that three-body recombination can maintain a steady state. Departures from a Maxwellian distribution of the free-electrons were found to have a negligible effect on the predicted steady-state characteristics, at least for the case of a nitrogen plasma.

The feasibility of such nonequilibrium discharges was demonstrated in atmospheric-pressure nitrogen and air at both room temperature and around 2000K with electrode spacings of cm scale. Stable, diffuse DC discharges have been achieved at atmospheric pressure for a range of gas flow and temperature conditions including those which produce n_e of 10^{12} to 10^{13} cm^{-3} without significant gas heating. Good agreement between theoretical and measured discharge characteristics has been obtained for both air and nitrogen discharges over a wide range of conditions including electron densities greater than 10^{12} in air and 10^{13} in nitrogen.

The good agreement between the predictions of the two-temperature chemistry model and the measured discharge characteristics provides validation of the proposed

10

mechanism of ionization in two-temperature air and nitrogen plasmas. These results enabled us to propose a repetitively pulsing strategy with ultrashort (10 ns) high voltage pulses, as a way to reduce the power required to produce electron densities in excess of 10^{12} cm^{-3} in atmospheric pressure air. Both single-shot and repetitively pulsed diffuse discharges at 100 kHz have been demonstrated (refs. 7-9), with power reductions of over two orders of magnitude for average electron densities greater than 10^{12} cm^{-3}.

4. AASERT Students Supported by this Grant

- Richard J. Gessman, Graduate Research Assistant, Ph.D. 2000, Stanford University.

- Edward Wahl, Graduate Research Assistant, Ph.D. 2001, Stanford University.

- Kate Snyder, Graduate Research Assistant, Ph.D. 2002 (expected), Stanford University.

- Jonathan Flad, Graduate Research Assistant, Ph.D. 2002 (expected), Stanford University.

5. References

1. E.E. Kunhardt. *IEEE Trans. Plasma Science.* **28**, 189-200 (2000).
2. L. Pierrot, C.O. Laux, C.H. Kruger. *Prog. Plas. Proc. Mat.* Begell House, NY, 153-159 (1999).
3. L. Pierrot, L. Yu, R. J. Gessman, C.O. Laux, C.H. Kruger. *AIAA 99-3478*, 30th PDL Conf., Norfolk, VA (1999).
4. L. Yu, L. Pierrot, C. O. Laux, C.H. Kruger. *Plasma Chem. Plasma Proc.* **21**, 483-503 (2001).
5. R.J. Kee, F.M. Rupley, J.A. Miller. *CHEMKIN-II.* Sandia Report SAND89-8009 (1989).
6. C.O. Laux, L. Yu, D.M. Packan, R.J. Gessman, L. Pierrot, C.H. Kruger, R.N. Zare. *AIAA 99-3476*, 30th PDL Conf., Norfolk, VA (1999).
7. M. Nagulapally, G.V. Candler, C.O. Laux, L. Yu, D. Packan, C.H. Kruger, R. Stark, K.H. Schoenbach, AIAA 00-2417, 31st PDL Conf., Denver, CO, 2000.
8. D. Packan, L. Yu, C.O. Laux, C.H. Kruger, "Repetitively-Pulsed DC Glow Discharge in Atmospheric Pressure Air: Modeling and Experiments with a 12 kV, 10 ns, 100 kHz Pulse Generator," Proceedings of the 28th IEEE International Conference on Plasma Science, p. 259, Las Vegas, NV, June 17-22, 2001.
9. C.H. Kruger, C.O. Laux, L. Yu, D.M. Packan, L. Pierrot, *Pure and Applied Chemistry*, Vol. 74, No. 3, pp. 337-347, March 2002.